



Oxysulfide LiAlSO: A Lithium Superionic Conductor from First Principles

Xuelong Wang,^{1,2} Ruijuan Xiao,^{1,*} Hong Li,¹ and Liquan Chen¹

¹Beijing National Laboratory for Condensed Matter Physics, Institute of Physics, Chinese Academy of Sciences, Beijing 100190, China

²University of Chinese Academy of Sciences, Beijing 100049, China

(Received 23 January 2017; published 12 May 2017)

Through first-principles calculations and crystal structure prediction techniques, we identify a new layered oxysulfide LiAlSO in orthorhombic structure as a novel lithium superionic conductor. Two kinds of stacking sequences of layers of AlS_2O_2 are found in different temperature ranges. Phonon and molecular dynamics simulations verify their dynamic stabilities, and wide band gaps up to 5.6 eV are found by electronic structure calculations. The lithium migration energy barrier simulations reveal the collective interstitial-host ion “kick-off” hopping mode with barriers lower than 50 meV as the dominating conduction mechanism for LiAlSO, indicating it to be a promising solid-state electrolyte in lithium secondary batteries with fast ionic conductivity and a wide electrochemical window. This is a first attempt in which the lithium superionic conductors are designed by the crystal structure prediction method and may help explore other mixed-anion battery materials.

DOI: 10.1103/PhysRevLett.118.195901

Searching for lithium superionic conductors has continuously attracted a lot of attention over the past few decades, especially regarding the development of all-solid-state lithium batteries [1]. By replacing the liquid electrolytes containing flammable organic solvents currently used in lithium ion batteries, inorganic solid electrolytes (SEs) are expected to avoid the problems of leakage, vaporization, and decomposition, exhibit fewer side reactions, and have higher safety [2,3]. However, high ionic conductivities comparable to those of organic liquid electrolytes ($\sim 10^{-2}$ S/cm at room temperature) are rarely found in solids. Designing new lithium superionic conductors is of major importance to current solid-state lithium battery devices.

At present, the only kinds of solid materials with ionic conductivity in the order of 10^{-2} S/cm at room temperature are $\text{Li}_{10}\text{GeP}_2\text{S}_{12}$ [4] and its derivatives $\text{Li}_{10}\text{MP}_2\text{X}_{12}$ ($M = \text{Ge, Sn, Si, ...}; X = \text{S, Se, ...}$) [5,6], the $\text{Li}_7\text{P}_3\text{S}_{11}$ glass ceramics [7], and the aliovalent-ion doping system $\text{Li}_{9.54}\text{Si}_{1.74}\text{P}_{1.44}\text{S}_{11.7}\text{Cl}_{0.3}$ [8]. Although they have impressively high ionic conductivity, sulfides generally suffer from high sensitive to moisture [9] and poor stability of sulfide solid electrolyte-oxide cathode interfaces [10]. Compared with sulfides, the oxide SEs have significantly better chemical and electrochemical stability [11], though the highest ionic conductivity achieved in oxide SEs is still 1 order of magnitude lower than those of liquid electrolytes [12]. To combine the advantages of sulfides and oxides, we previously proposed to improve the stability and lithium ionic conductivity by O-doping in sulfide SEs, $\beta\text{-Li}_3\text{PS}_4$ [13,14]. Experimental evidence is provided in $75\text{Li}_2\text{S} \cdot (25-x)\text{P}_2\text{S}_5 \cdot x\text{P}_2\text{O}_5$ oxysulfide glass-ceramic electrolytes by Xu *et al.* [15]. Thus, anion mixing is expected to be a promising strategy to design the lithium superionic conductors with improved stabilities and high ionic conductivity [11,13,14]. Discovering oxysulfide superionic

conductors may combine the extremely high ionic conductivity of sulfides with the excellent stability of oxides.

It is not uncommon for oxysulfide compounds to be found in various applications. For example, rare-earth oxysulfides have technological importance because of their exceptional luminescent efficiencies [16], and bulk superconductivity has been identified in bismuth and copper oxysulfides [17]. Transition-metal-based oxysulfides act as photocatalysts in the decomposition of water [18]. LaCuOS - and MZnOS -layered ($M = \text{Ca, Ba}$) oxysulfides have been synthesized and shown to act as wide-band-gap semiconductors applied in solar cells [19]. There have also been a few attempts to apply this kind of material to lithium ion batteries: oxysulfide glasses prepared by rapid quenching have been tested as solid electrolytes, additions, and coatings [20,21], and $\text{V}_2\text{S}_4\text{O}$ [22], TiO_yS_z [23], layered $\text{LiNiS}_y\text{O}_{2-y}$ [24], and spinel $\text{Li}_{1.03}\text{Al}_{0.2}\text{Mn}_{1.8}\text{O}_{3.96}\text{S}_{0.04}$ [25] have been developed as new positive electrodes. To the best of our knowledge, there has been still no discovery of a crystalline oxysulfide for SEs used in lithium batteries.

In recent years, assisted by improvements in the method of crystal structure prediction [26,27], some new materials, including topological insulators [28], superhard materials [29], superconductors [30], and so forth, have been predicted from scratch. Stable or metastable structures can be determined at given chemical compositions from first-principles calculations, which is an efficient way of helping the design of multifunctional materials. In this Letter, we identify by first-principles calculations a new lithium superionic conductor, LiAlSO, with tetrahedral coordination of the cations in orthorhombic structure. This new structure, with eight atoms in a unit cell, can be regarded as a modification of orthorhombic $\beta\text{-NaFeO}_2$ with some sites exchanging between univalent and trivalent ions and

the co-occupation of anion sites by O and S. Total energy calculations at 0 K indicate its energetic stability with respect to possible binary decomposition products ($\text{Li}_2\text{S} + \text{Li}_2\text{O} + \text{Al}_2\text{O}_3 + \text{Al}_2\text{S}_3$). Two kinds of stacking sequences of AlS_2O_2 layers are found in different temperature ranges, and their dynamic stabilities are verified by phonon calculations and molecular dynamic simulations. Electronic band structure analysis shows that both structures are insulators with band-gap energy up to ~ 5.6 eV, which ensures the wide electrochemical window of this material. The most exciting finding is that the activation energies of Li ions migration are less than 50 meV along the a direction and the sliding of AlS_2O_2 layer shows no detriment to Li^+ hopping; this indicates the superionic conductivity and novel transport properties in this compound. These results establish the first superionic conductor designed from scratch and reveal the remarkable potential of oxysulfides applied as solid electrolytes in lithium batteries.

The crystal structure of LiAlSO was predicted by the particle-swarm optimization method as implemented in the CALYPSO code [31], which has successfully predicted various new structures [28]. The energy minimization was performed by the density functional theory (DFT) method with the Vienna *ab initio* simulation package (VASP) [32]. A generalized gradient approximation (GGA) with a parameterized exchange-correlation functional according to Perdew, Burke, and Ernzerhof (PBE) [33] is adopted in the DFT calculations. The cutoff for the wave function is specified as 500 eV and the k -mesh used to sample the Brillouin zone has a density of 1 point per 0.06 \AA^{-3} . Both ions and cells are relaxed in the optimization with the energy and force convergence criterion of 10^{-5} eV and 0.002 eV/\AA , respectively. The migration barrier of Li ion is obtained using a supercell with 32 formula units (f.u.) by the nudged elastic band (NEB) method as implemented in VASP [34]. Both the vacancy-assisted and the interstitial-assisted hopping mechanisms are considered for each diffusion pathway; thus, one Li ion is removed from or added into the supercell and the charge neutrality of the system is maintained by a uniform background opposite charge. Each image structure is relaxed until the forces felt by each atom are less than 0.02 eV/\AA . Phonon calculations are performed using the phonopy package [35]. Electronic structures are calculated using the modified Becke-Johnson exchange potential (MBJ) in combination with the local-density approximation (LDA) correlation to obtain more accurate band gaps [36]. The first-principles molecular dynamics (FPMD) is also carried out on the supercell with 32 f.u. A Nose-Hoover thermostat was adopted for the simulations with the temperature of 300–1500 K, lasting for 12 000 steps with a time step of 1 fs. The first 2 ps are used to equilibrate the system at the temperature, and the structural information is extracted from the last 10 000 steps.

The predicted LiAlSO crystallizes in orthorhombic space group $Pmc2_1$ with lattice parameters of $a = 3.5811 \text{ \AA}$,

$b = 6.5132 \text{ \AA}$, and $c = 5.3166 \text{ \AA}$, as shown in Fig. 1. The Li, Al, S, and O atoms occupy Wyckoff positions at $2a(0.000, 0.284, 0.121)$, $2b(0.500, 0.124, 0.529)$, $2a(0.000, 0.313, 0.647)$, and $2b(0.500, 0.113, 0.194)$, respectively. Each Li or Al atom coordinates to two oxygen atoms and two sulfur atoms, forming a tetrahedral environment. AlS_2O_2 tetrahedra are connected to each other by a shared corner to form layers in the ac plane. The AlS_2O_2 planes stack layer by layer along the b direction separated by severely distorted LiS_2O_2 tetrahedra. The Al-S and Al-O distances are 2.260 \AA and 1.779 \AA , respectively, which are the regular bond lengths found in tetrahedral-coordinated LiAlO_2 and LiAlS_2 [37]. The lengths of the Li-S and Li-O bonds are 2.577 \AA and 2.147 \AA , respectively; these are more than 5% larger than those in LiAlO_2 and LiAlS_2 , indicating the weaker constraints on Li ions in this compound.

The total energy calculations are adopted to evaluate the thermodynamic stability at 0 K for the crystal structure determined above. Considering that many different decomposition reactions can be defined for this compound, the stabilities with respect to decompositions into binaries and ternaries are chosen and the corresponding decomposition reactions are assumed as follows:

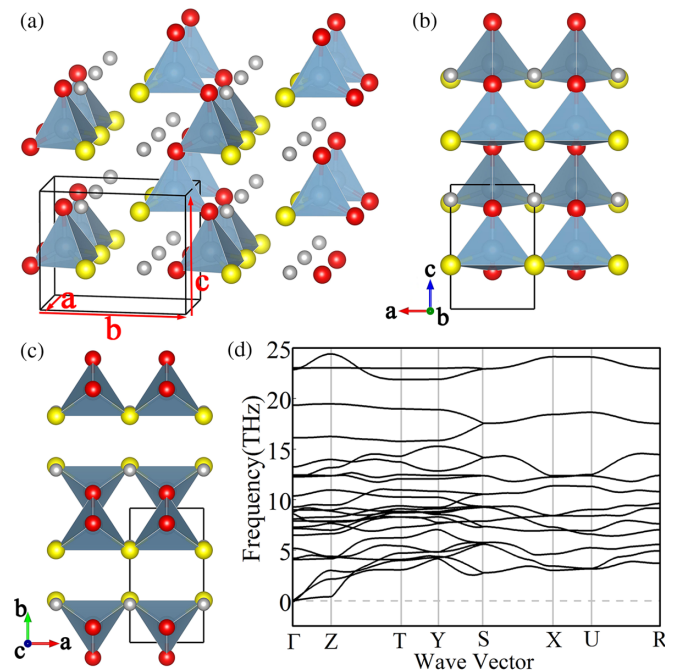
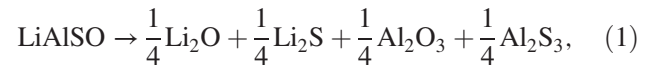
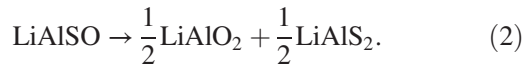


FIG. 1. Crystal structure of $Pmc2_1\text{LiAlSO}$ and its phonon dispersion. (a) A polyhedral view of the predicted structure and the views along the (b) b and (c) c crystal axis. (d) Calculated phonon dispersion curves of $Pmc2_1\text{LiAlSO}$. The grey, yellow, and red spheres represent the Li, S, and O atoms, respectively. The dark blue tetrahedron stands for the AlS_2O_2 unit.



By using the structures of the related binaries and ternaries taken from the Inorganic Crystal Structure Database [38], the calculations provide the reaction energy of 114 meV/atom for Eq. (1), indicating that it is possible to stabilize LiAlSO and to synthesize it from the parent binary phases. However, the calculated reaction energy of Eq. (2) is -46 meV/atom, indicating that the predicted LiAlSO phase is thermodynamically unstable at 0 K with respect to LiAlO_2 and LiAlS_2 . Nevertheless, the energy of LiAlSO decomposing into these two ternary competing phases is relatively low, implying that it can exist as a metastable structure or be stabilized by entropic effects, as the newly discovered Li superionic conductor $\text{Li}_{10}\text{GeP}_2\text{S}_{12}$ [39] and its derivatives $\text{Li}_{10}\text{MP}_2\text{X}_{12}$ ($M = \text{Ge, Sn, Si, \dots}$; $X = \text{S, Se, \dots}$) [6]. The estimation of entropic contributions is discussed in the Supplemental Material [40].

We now characterize the phonon distribution of $Pmc2_1\text{LiAlSO}$ and obtain the results as shown in Fig. 1(d). The absence of imaginary frequency modes in the Brillouin zone confirms the dynamic stability of this new structure. A flat phonon mode ranging from 0 to 0.38 THz (1.57 meV) has been observed for the high-symmetry direction of Γ -Z. It is mainly composed of the collective vibration of the AlS_2O_2 layer along the a axis. This mode becomes dispersionless, indicating the tendency of the AlS_2O_2 layer to slip with small external driving force. FPMD simulations within the temperature range of 300–1500 K show that the slip activities with a shift of $1/2a$ are completed in the first 2 ps and the new structure with $1/2a$ sliding of the AlS_2O_2 layer is maintained in the last 10 ps. By averaging the atomic positions of the last 10 ps from the FPMD simulations, the new structure, which is orthorhombic with the space group of $Cmc2_1$, is identified [Fig. 2(a)]. The averaged mean-squared displacements (MSDs) from FPMD simulations at 1500 K for the

last 10 ps show that after transforming into the new phase the instantaneous MSDs for Al, S, and O atoms have constant small values near zero [Fig. 2(b)]. The oscillations of Al, S, and O atoms with respect to their original equilibrium positions without any migrations indicate that the host structure of LiAlSO in $Cmc2_1$ symmetry is stable and no more structural changes are found. Compared with the $Pmc2_1$ phase, the Al-S and Al-O distances in $Cmc2_1\text{LiAlSO}$ barely change, becoming 2.260 Å and 1.769 Å, respectively. At the same time, the Li-S distance shrinks to 2.527 Å while the Li-O distance expands a little to 2.153 Å, indicating that the constraints on Li ions are still weak in the sliding phase. The calculated energy of $Pmc2_1$ phase is only 10.8 meV/f.u. lower than that of the $Cmc2_1$ phase at 0 K. To understand the phase transition, the total energy calculations are performed for a series of different sliding distances of AlS_2O_2 layers along the a axis from the original position in the $Cmc2_1$ structure. The obtained energy variation is less than 1 meV/f.u. even when the sliding distance reaches 0.2 Å, proving a very flat energy landscape. Therefore, the Gibbs energy of the $Cmc2_1$ phase at finite temperature can be estimated with quasiharmonic approximation [44]. Thus, the upper bound of the phase-transform temperature is estimated as ~ 265 K, suggested by the Gibbs free energy difference between the $Pmc2_1$ and $Cmc2_1$ phases shown in Fig. 2(c). Reaction free-energy calculations show that LiAlSO in $Cmc2_1$ symmetry becomes thermodynamically stable with respect to LiAlS_2 and LiAlO_2 at relatively high temperature and pressure, which provides the possibility to synthesize this new structure (see the Supplemental Material [40] for details). The exfoliation energy of $Pmc2_1$ and $Cmc2_1\text{LiAlSO}$ along the (010) surface are estimated to be 116 mJ/m² and 90 mJ/m², respectively, using the same method in Ref. [45]. These values are slightly lower than but comparable to the exfoliation energy of graphite, 143 mJ/m² [45]. Thus, we expect that the utilization of LiAlSO will not be hindered by mechanical stability. In other words, LiAlSO is predicted to be dynamically stable

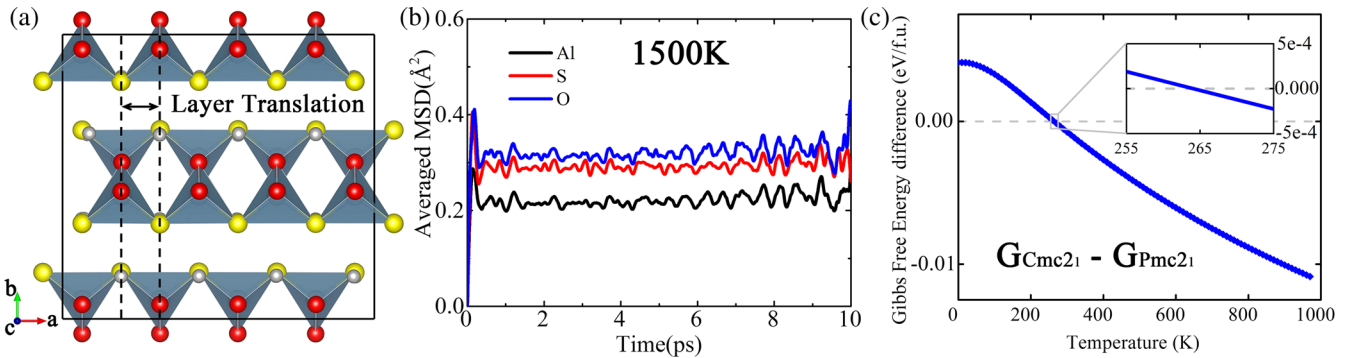


FIG. 2. (a) Average structure of a pristine LiAlSO supercell from FPMD simulations at $T = 800$ K for the last 10 ps. (b) The averaged MSDs for Al, S, and O atoms from FPMD simulations at 1500 K for last 10 ps. (c) The difference of Gibbs free energy between $Pmc2_1$ and $Cmc2_1\text{LiAlSO}$ as a function of temperature.

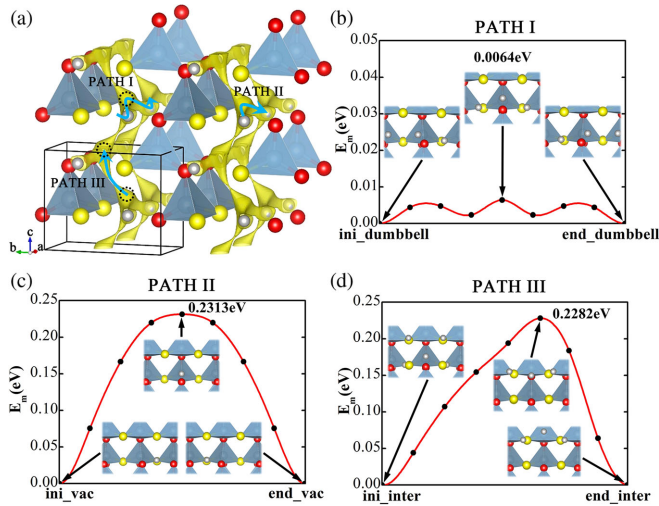


FIG. 3. The calculated kinetic properties of $Pmc2_1LiAlSO$. (a) The continuous Li^+ migration channels determined by the BV-based method, and the energy barriers simulated by the NEB method for (b) the kick-off mechanism along the a direction, (c) the direct vacancy hopping along the a axis, and (d) the interstitial Li^+ hopping along the c axis. The interstitial sites related to the Li^+ migration are marked by dotted circles. The local atomic configurations of initial, transition, and final states calculated with the NEB method are shown as insets. The initial and final structures of each pathway are labeled on the horizontal axis as “ini_” and “end_”, respectively. The labels “dumbbell”, “vac,” and “inter” represent the dumbbell, vacancy, and interstitial configuration, respectively.

in a large temperature range with two different kinds of AlS_2O_2 -layer stacking styles.

Having determined both the thermal and dynamic stabilities of $LiAlSO$, we turn to the study of Li^+ transport properties. First, the quasiempirical bond-valence (BV) method with high calculation efficiency [13,46] is employed to obtain the initial knowledge of possible ionic transportation channels and interstitial sites of the new structures. Figures 3(a) and 4(a) demonstrate the isosurfaces of potential energies calculated by BV-based method, which are considered as the continuous network for Li^+ ion transport. An interstitial $2b$ site was found in the $Pmc2_1$ structure and a $4a$ interstitial site in the $Cmc2_1$ structure. The interstitial sites related to Li^+ migration are marked by dotted circles in Figs. 3(a) and 4(a). In the $Pmc2_1$ phase, the channels are connecting Li^+ ions between two adjacent AlS_2O_2 layers by interstitial sites. The continuous pathways are formed along both the a and c axes. The migration path in the c direction becomes hampered in the $Cmc2_1$ structure because of the stacking sequence of the neighboring AlS_2O_2 layers has changed; however, the Li^+ transport through interstitial sites in the a direction are still quite unobstructed. In both cases, the paths traveling throughout the lattice along the b direction are prohibited because it would cost too much energy for Li^+ to penetrate the AlS_2O_2 layers.

To further understand the kinetic properties revealed by the BV method, the simulations using DFT in combination with the NEB method [34] are conducted carefully to obtain activation energies for different hopping pathways. Because both interstitials and vacancies are possible current carriers in solid electrolytes, three different hopping mechanisms are considered, namely, vacancies of Li ion directly hopping between Li sites, interstitial Li ions directly hopping between empty interstitial sites, and the so-called “kick-off” collective hopping mode with an interstitial Li ion pulling away the neighbor host Li ion into the next interstitial site and occupying the lattice site itself [47]. For the $Pmc2_1$ structure, the calculated barrier shapes and corresponding activation energies are shown in Figs. 3(b)–3(d). The Li ions hopping along the a axis with a kick-off mechanism is found to be the easiest ionic conduction pathway in the $Pmc2_1$ structure. When an extra Li ion is added to the $Pmc2_1$ structure, the configuration of Li ions with the lowest energy is not the extra Li ion staying exactly at the interstitial site but two Li ions posing like a dumbbell centering at an empty lattice site, as shown in the inset of Fig. 3(b). In this situation, one extra Li ion staying at the interstitial site is the transition state with an extremely low energy barrier of 6.4 meV. The direct vacancy hopping along the a axis is also a migration with a low barrier of 0.231 eV. Along the c direction, the favorite pathway is the hopping of an interstitial Li ion directly between two interstitial sites with an energy barrier of 0.228 eV, comparable to the barrier of vacancy hopping along the a axis in the same phase. Therefore, a two-dimensional transporting network with low energy barriers could form in the ac plane in the $Pmc2_1$ structure. After transforming into the $Cmc2_1$ phase, the Li ion migration along the a axis with a kick-off mechanism is still the energetically most favorable pathway, as shown in Fig. 4(b). The energy barrier of the kick-off mechanism is only 47.2 meV, which is much lower than the values of many known solid electrolytes [48–50]. Different from the hopping in the $Pmc2_1$ structure shown in Fig. 3(b), the dumbbell configuration acts as the transition state. The direct vacancy hopping along the a axis given in Fig. 4(c) is a mechanism with a low barrier of 0.140 eV, which is even lower than the barrier of the same path in the $Pmc2_1$ structure. However, the slide of AlS_2O_2 layers along the a axis varies the interlayer hopping step of the $Cmc2_1$ structure. As shown in Fig. 4(d), in the $Cmc2_1$ phase the interlayer hopping mode with the relatively lowest barrier is the interlayer kick-off with an activation energy of 0.705 eV, which is much higher than that of jumping along the a axis in the same structure. Thus, one-dimensional transportation behavior should be expected in the $Cmc2_1$ structure and the fast ionic conducting channel is in the a direction. With an ultralow energy barrier along the a axis in a kick-off transport mode, $LiAlSO$ in both the $Pmc2_1$ and $Cmc2_1$ phases are predicted to be excellent fast ionic conductors, satisfying the first

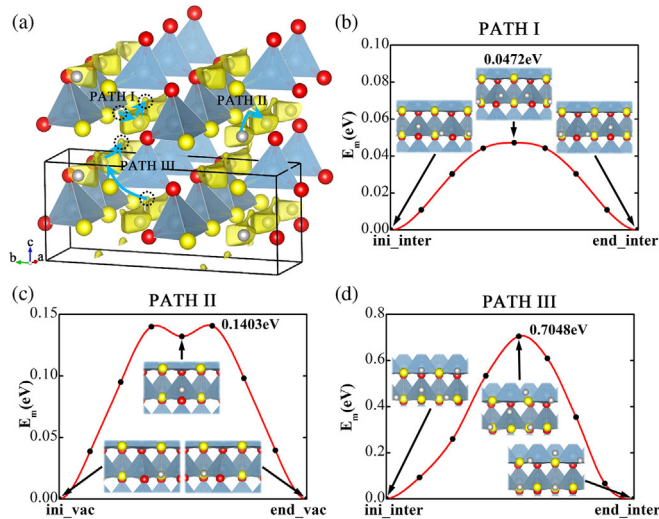


FIG. 4. The calculated kinetic properties of $Cmc2_1LiAlSO$. (a) The continuous Li^+ migration channels determined by the BV-based method, and the energy barriers simulated by the NEB method for (b) the kick-off mechanism along the a direction, (c) the direct vacancy hopping along the a axis, and (d) the kick-off mechanism along the c axis. Symbols and labels have the same meaning as Fig. 3.

important prerequisite for solid electrolytes with appropriate performance.

As an electrolyte, an adequate band gap for negligible electronic conductivity is undoubtedly important to ensure the electronic structure stability and to prevent self-discharge. Therefore, further calculations based on DFT are in process to obtain the electronic structures of $LiAlSO$. Considering that a GGA-type functional like PBE usually underestimates the band gap of insulators, calculations with the MBJ exchange potentials in combination with LDA correlation [36], which has been shown to offer band gaps with an accuracy similar to that of hybrid functional [51], are conducted. Results show that the band gaps for the $Pmc2_1$ and $Cmc2_1$ phases are 5.60 eV and 5.76 eV, respectively, suggesting that both phases are insulators and supposedly provide wide electrochemical windows. Besides the wide band gap, the alignment of valence and conduction bands of $LiAlSO$ with respect to those of Li metal and $LiCoO_2$ cathodes further indicates the electrochemical stability of this oxysulfide system (see the Supplemental Material [40] for details).

In summary, by means of first-principles calculations we have discovered oxysulfide $LiAlSO$, a new lithium superionic conductor in orthorhombic structure with chemical bonding in tetrahedral networks. The structure is composed of stacking layers of AlS_2O_2 tetrahedrons sharing vertex atoms with Li ions located between neighboring layers. The stacking sequence of AlS_2O_2 changes by sliding one AlS_2O_2 layer along the a axis with half a lattice vector if the temperature is above ~ 265 K, which alters the space

group from $Pmc2_1$ to $Cmc2_1$. The dynamic stability of $Pmc2_1LiAlSO$ is verified by phonon spectrum analysis, and that of $Cmc2_1LiAlSO$ is confirmed by FPMD simulations. NEB calculations reveal that the collective interstitial-host ion kick-off hopping mode is the dominant conduction mechanism, with barriers lower than 50 meV for both $Pmc2_1$ and $Cmc2_1LiAlSO$; this makes this material a promising fast ionic conductor. The electronic structure calculations indicate that both structures are insulators with a wide band gap of up to 5.6 eV, ensuring that they are expected to produce wide electrochemical windows as solid-state electrolytes in lithium secondary batteries. Therefore, relatively good ionic kinetic properties and wide electrochemical windows can be expected in a large temperature range for $LiAlSO$, which should provide a promising option for solid electrolyte or electrode coating material. Our findings represent a significant advance in oxysulfides and should promote further exploration of this class of materials. It is a first attempt in which the lithium superionic conductors are designed by the crystal structure prediction method. This Letter serves as an exemplary case study of theoretically designing lithium superionic conductors from scratch, and it may help to explore other complex oxysulfides and mixed-anion compounds.

We acknowledge the National Natural Science Foundation of China (Grant No. 11234013), “863” Project (Grant No. 2015AA034201), the Beijing S&T Project (Grant No. D161100002416003), and the Youth Innovation Promotion Association (Grant No. 2016005) for financial support, as well as the Shanghai Supercomputer Center for providing computing resources. We would like to express our thanks to Prof. Jiawang Hong (Beijing Institute of Technology) for fruitful discussion.

*Corresponding author.
rjxiao@iphy.ac.cn

- [1] P. Knauth, *Solid State Ionics* **180**, 911 (2009).
- [2] K. Takada, *Acta Mater.* **61**, 759 (2013).
- [3] X. Yao, B. Huang, J. Yin, G. Peng, Z. Huang, C. Gao, D. Liu, and X. Xu, *Chin. Phys. B* **25**, 018802 (2016).
- [4] N. Kamaya *et al.*, *Nat. Mater.* **10**, 682 (2011).
- [5] P. Bron, S. Johansson, K. Zick, J. Schmedt auf der Gunne, S. Dehnen, and B. Roling, *J. Am. Chem. Soc.* **135**, 15694 (2013).
- [6] S. P. Ong, Y. Mo, W. D. Richards, L. Miara, H. S. Lee, and G. Ceder, *Energy Environ. Sci.* **6**, 148 (2013).
- [7] Y. Seino, T. Ota, K. Takada, A. Hayashi, and M. Tatsumisago, *Energy Environ. Sci.* **7**, 627 (2014).
- [8] Y. Kato, S. Hori, T. Saito, K. Suzuki, M. Hirayama, A. Mitsui, M. Yonemura, H. Iba, and R. Kanno, *Nat. Energy* **1**, 16030 (2016).
- [9] H. Muramatsu, A. Hayashi, T. Ohtomo, S. Hama, and M. Tatsumisago, *Solid State Ionics* **182**, 116 (2011).
- [10] F. Han, Y. Zhu, X. He, Y. Mo, and C. Wang, *Adv. Energy Mater.* **6**, 1501590 (2016).

- [11] Y. Zhu, X. He, and Y. Mo, *J. Mater. Chem. A* **4**, 3253 (2016).
- [12] M. Tatsumisago, M. Nagao, and A. Hayashi, *J. Asian Ceram. Soc.* **1**, 17 (2013).
- [13] R. Xiao, H. Li, and L. Chen, *Sci. Rep.* **5**, 14227 (2015).
- [14] X. Wang, R. Xiao, H. Li, and L. Chen, *Phys. Chem. Chem. Phys.* **18**, 21269 (2016).
- [15] Y. Tao, S. Chen, D. Liu, G. Peng, X. Yao, and X. Xu, *J. Electrochem. Soc.* **163**, A96 (2016).
- [16] L. E. Sobon, *J. Appl. Phys.* **42**, 3049 (1971).
- [17] C.-H. Yee, T. Birol, and G. Kotliar, *Europhys. Lett.* **111**, 17002 (2015).
- [18] A. Ishikawa, T. Takata, J. N. Kondo, M. Hara, H. Kobayashi, and K. Domen, *J. Am. Chem. Soc.* **124**, 13547 (2002).
- [19] T. Sambrook, C. F. Smura, S. J. Clarke, K. M. Ok, and P. S. Halasyamani, *Inorg. Chem.* **46**, 2571 (2007).
- [20] K. Takada, N. Aotani, K. Iwamoto, and S. Kondo, *Solid State Ionics* **86–88**, 877 (1996).
- [21] H. Takahara, T. Takeuchi, M. Tabuchi, H. Kageyama, Y. Kobayashi, Y. Kurisu, S. Kondo, and R. Kanno, *J. Electrochem. Soc.* **151**, A1539 (2004).
- [22] G. Tchangbedji, D. A. Odink, and G. Ouyard, *J. Power Sources* **44**, 577 (1993).
- [23] B. Fleutot, B. Pecquenard, F. Le Cras, B. Delis, H. Martinez, L. Dupont, and D. Guy-Bouyssou, *J. Power Sources* **196**, 10289 (2011).
- [24] S. H. Park, Y. K. Sun, K. S. Park, K. S. Nahm, Y. S. Lee, and M. Yoshio, *Electrochim. Acta* **47**, 1721 (2002).
- [25] Y. K. Sun and I. H. Oh, *J. Power Sources* **94**, 132 (2001).
- [26] Y. Wang, J. Lv, L. Zhu, and Y. Ma, *Comput. Phys. Commun.* **183**, 2063 (2012).
- [27] C. W. Glass, A. R. Oganov, and N. Hansen, *Comput. Phys. Commun.* **175**, 713 (2006).
- [28] Y. Chen *et al.*, *J. Phys. Chem. C* **117**, 25677 (2013).
- [29] X. Zhang, Y. Wang, J. Lv, C. Zhu, Q. Li, M. Zhang, Q. Li, and Y. Ma, *J. Chem. Phys.* **138**, 114101 (2013).
- [30] X. Zhong, H. Wang, J. Zhang, H. Liu, S. Zhang, H. F. Song, G. Yang, L. Zhang, and Y. Ma, *Phys. Rev. Lett.* **116**, 057002 (2016).
- [31] Y. Wang, J. Lv, L. Zhu, and Y. Ma, *Phys. Rev. B* **82**, 094116 (2010).
- [32] G. Kresse and J. Furthmuller, *Comput. Mater. Sci.* **6**, 15 (1996).
- [33] J. P. Perdew, K. Burke, and M. Ernzerhof, *Phys. Rev. Lett.* **77**, 3865 (1996).
- [34] G. Henkelman and H. Jónsson, *J. Chem. Phys.* **113**, 9978 (2000).
- [35] A. Togo and I. Tanaka, *Scr. Mater.* **108**, 1 (2015).
- [36] A. D. Becke and E. R. Johnson, *J. Chem. Phys.* **124**, 221101 (2006).
- [37] E. E. Hellstrom and R. A. Huggins, *Mater. Res. Bull.* **14**, 881 (1979).
- [38] Inorganic Crystal Structure Database, Fachinformationszentrum. Karlsruhe: ICSD (2008) <https://icsd.fiz-karlsruhe.de/search/basic.xhtml>.
- [39] Y. Mo, S. P. Ong, and G. Ceder, *Chem. Mater.* **24**, 15 (2012).
- [40] See Supplemental Material at <http://link.aps.org/supplemental/10.1103/PhysRevLett.118.195901> for detailed information about the estimation of entropic contributions to the Gibbs free-energy and the analysis on SE's electrochemical stability relative to cathode material and Li metal, which includes Refs. [41–43].
- [41] N. E. Singh-Miller and N. Marzari, *Phys. Rev. B* **80**, 235407 (2009).
- [42] A. Van der Ven, M. K. Aydinol, G. Ceder, G. Kresse, and J. Hafner, *Phys. Rev. B* **58**, 2975 (1998).
- [43] J. van Elp, J. L. Wieland, H. Eskes, P. Kuiper, G. A. Sawatzky, F. M. F. de Groot, and T. S. Turner, *Phys. Rev. B* **44**, 6090 (1991).
- [44] M.-H. Chen, A. Emly, and A. Van der Ven, *Phys. Rev. B* **91**, 214306 (2015).
- [45] R. Rasuli and A. I. Zad, *Appl. Surf. Sci.* **256**, 7596 (2010).
- [46] S. Adams and R. P. Rao, *Phys. Status Solidi (a)* **208**, 1746 (2011).
- [47] S. Shi, Y. Qi, H. Li, and L. G. Hector, *J. Phys. Chem. C* **117**, 8579 (2013).
- [48] W. Xia, B. Xu, H. Duan, Y. Guo, H. Kang, H. Li, and H. Liu, *ACS Appl. Mater. Interfaces* **8**, 5335 (2016).
- [49] H. Buschmann *et al.*, *Phys. Chem. Chem. Phys.* **13**, 19378 (2011).
- [50] M. Monchak, T. Hupfer, A. Senyshyn, H. Boysen, D. Chernyshov, T. Hansen, K. G. Schell, E. C. Bucharsky, M. J. Hoffmann, and H. Ehrenberg, *Inorg. Chem.* **55**, 2941 (2016).
- [51] F. Tran and P. Blaha, *Phys. Rev. Lett.* **102**, 226401 (2009).